

# Giant Flare in SGR 1806-20 and Its Compton Reflection from the Moon

D. D. Frederiks<sup>1</sup>, S. V. Golenetskii<sup>1</sup>, V. D. Palshin<sup>1</sup>, R. L. Aptekar<sup>1</sup>, V. N. Ilyinskii<sup>1</sup>,  
F. P. Oleinik<sup>1</sup>, E. P. Mazets<sup>1</sup>, and T. L. Cline<sup>2</sup>

## ABSTRACT

We analyze the data obtained when the Konus-Wind gamma-ray spectrometer detected a giant flare in SGR 1806-20 on December 27, 2004. The flare is similar in appearance to the two known flares in SGR 0526-66 and SGR 1900+14 while exceeding them significantly in intensity. The enormous X-ray and gamma-ray flux in the narrow initial pulse of the flare leads to almost instantaneous deep saturation of the gamma-ray detectors, ruling out the possibility of directly measuring the intensity, time profile, and energy spectrum of the initial pulse. In this situation, the detection of an attenuated signal of Compton back-scattering of the initial pulse emission by the Moon with the Helicon gamma-ray spectrometer onboard the Coronas-F satellite was an extremely favorable circumstance. Analysis of this signal has yielded the most reliable temporal, energy, and spectral characteristics of the pulse. The temporal and spectral characteristics of the pulsating flare tail have been determined from Konus-Wind data. Its soft spectra have been found to contain also a hard power-law component extending to 10 MeV. A weak afterglow of SGR 1806-20 decaying over several hours is traceable up to 1 MeV. We also consider the overall picture of activity of SGR 1806-20 in the emission of recurrent bursts before and after the giant flare.

*Subject headings:* neutron stars, flares, gamma rays, Compton scattering

## INTRODUCTION

The first two soft gamma repeaters, SGR 0526-66 (Mazets et al. 1979a; Golenteskii et al. 1984) and SGR 1900+14 (Mazets et al. 1979b), were discovered and localized in March 1979. The third SGR 1806-20 was discovered in 1983 (Atteia et al. 1987; Laros et al. 1987). And only in 1998 was the fourth SGR 1627-41 discovered (Woods et al. 1999). The situation with the possible fifth SGR 1801-23 (Cline et al. 2000) arouses scepticism, since only two soft bursts separated by an interval of several hours have been detected from this source.

The emission of recurrent bursts by the gamma repeaters is highly nonuniform in time. The

gamma repeaters are predominantly in quiescence. This phase can last for years, being interrupted by reactivation periods that can be very intense.

The temporal and spectral characteristics for all of the above gamma repeaters that have been observed over several years in the Konus-Wind experiment are summarized in a unified catalog of SGR activity (Aptekar et al. 2001).

Giant flares, very rare events comparable in peak emission power in the source ( $\sim 10^{45} - 10^{47}$  erg s<sup>-1</sup>) to the luminosity of quasars, are the second, incomparably more impressive type of SGR activity.

The giant flare of March 5, 1979, had remained a unique event for more than 19 years. On August 27, 1998, a giant flare came from SGR 1900+14. All the main features of the flare in SGR 0526-66 manifested themselves in this flare: a narrow, very intense initial emission peak with a hard energy spectrum accompanied by a rela-

<sup>1</sup>Ioffe Physico-Technical Institute, St.Petersburg, 194021, Russia; aptekar@mail.ioffe.ru

<sup>2</sup>Goddard Space Flight Center, NASA, Greenbelt, MD 20771, USA

tively weaker, spectrally soft tail that decayed for several minutes while pulsating (Mazets et al. 1999a; Hurley et al. 1999; Feroci et al. 1999). The third similar, but even more intense flare that came from SGR 1806-20 on December 27, 2004, was observed on many spacecraft equipped with X-ray and gamma-ray detectors: INTEGRAL, Mars Odyssey, Wind, Swift, RXTE, RHESSI, and others (Borkowski et al. 2004; Hurley et al. 2004; Mazets et al. 2004; Palmer et al. 2005; Hurley et al. 2005; Smith et al. 2005; Woods et al. 2005).

The enormous intensity of the initial pulse of the flare led to detector overload and saturation. As a result, the pulse time profile, spectrum, and intensity could not be measured reliably. These characteristics have been estimated more reliably by analyzing information from the small charged-particle detectors designed to study low-energy plasma and mounted on the Geotail (Terasawa et al. 2005), RHESSI, and Wind (Hurley et al. 2005) spacecraft.

In this paper, we consider in detail the results obtained in our Konus-Wind and Helicon-Coronas-F observations of the flare.

It should be noted that a peculiar giant flare was also observed in SGR 1627-41 on June 18, 1998. It differed in characteristics from the other three flares. The flare was a short single pulse with a hard, rapidly evolving spectrum, but it had no pulsating tail and was an order of magnitude less intense (Mazets et al. 1999b).

A joint analysis of the four gamma repeaters allows us to point out some features of their behavior on which we will dwell in the subsequent discussion.

Thompson and Duncan (1995, 1996) hypothesized that the soft gamma repeaters (SGRs) are young neutron stars with superstrong ( $\sim 10^{15}$  G) magnetic fields that rapidly spin down due to the losses through magnetodipole radiation.

## INSTRUMENTATION

The data considered here were obtained with the Konus gamma-ray spectrometer onboard the NASA Wind spacecraft and with the Helicon gamma-ray spectrometer onboard the Russian near-Earth Coronas-F spacecraft.

## Konus-Wind

The Konus-Wind gamma-ray spectrometer was described in detail by Aptekar et al. (1995).

For the convenience of the reader, let us briefly consider the main design features of the spectrometer. Two spectrometric gamma-ray detectors, S1 and S2, are placed on the spacecraft stabilized by rotation around the axis perpendicular to the plane of the ecliptic. Their axes are directed toward the south and north poles of the ecliptic, respectively, which ensures an all-sky survey. The two detectors operate independently of each other in two modes: background and burst ones. In the background mode, each detector measures the count rate with a resolution of 2.944 s in three energy windows (G1, G2, and G3), with the results being directly written to onboard memory. A trigger signal is generated when a burst is detected by a particular detector at time  $T_0$ . This signal triggers the burst mode in this detector. The burst time history is recorded in the G1, G2, and G3 windows in the time interval from  $T_0-0.512$  s to  $T_0+229.632$  s with a time resolution of 2, 16, 64, and 256 ms, which changes stepwise during the recording, and 64 multichannel spectra are measured in the energy range from 10 keV to 10 MeV with an accumulation time adapted to the current burst intensity. The changes in the time resolution as the time history is recorded are related to Konus telemetry capacity restrictions. The measurement results are written to the instrument's random access memory. On completion of the burst mode, the information is slowly rewritten to onboard memory, which takes 1–1.5 h. For the rewriting period, the instrument does not operate in the background mode. Clearly, in this scheme of operation, there is a risk of losing important information about the burst. Therefore, the instrument has two standby measuring systems. The first system records portions of the time history of a burst with a rapidly changing intensity of duration from 0.128 to 8.192 s with a resolution of 2 ms and saves information in random access memory if the recorded fast count rate variations are statistically significant. The second system continues to transmit the count rate measurements in the G2 window during the rewriting over the service telemetry channel with a resolution of 3.680 s. Note that both systems were used to record the giant flare.

## Helicon-Coronas-F

The Helicon gamma-ray spectrometer is one of the instruments onboard the Coronas-F solar space observatory (Oraevskii et al. 2002) that was placed in a near-Earth low-eccentricity polar orbit (orbital inclination 82°5, distance from the Earth 500–550 km) in June 2001. The spacecraft is stabilized by rotation around the axis directed toward the Sun with a 10' accuracy.

Helicon is designed to record solar flares, gamma-ray bursts, and SGR activity. The simultaneous operation of Helicon-Coronas-F and Konus-Wind makes it possible to perform a comparative analysis of the information about the same event from two instruments separated in space by a distance from several hundred thousand to  $\sim 2$  million kilometers. This increases the reliability of the observations of spectral and temporal features of the recorded emission and, in many cases, allows a fairly accurate triangulation of the sources to be performed. The Helicon gamma-ray spectrometer is similar to the Konus spectrometer in characteristics of its two detectors and in data presentation structure. One of its detectors is oriented toward the Sun and the other detector scans the antisolar hemisphere. The burst modes of operation of the two spectrometers are similar. The background mode of operation of Helicon was slightly modified. Eight energy windows in the range 10–200 keV are used to continuously monitor the hard X-ray emission from the Sun with a time resolution of 1 s. Additionally, the solar detector is equipped with a multichannel analyzer that continuously measures the energy spectra in the range 200 keV–10 MeV with an accumulation time of 32 s. The data are written to onboard memory without any interruptions in the measurements. Recall, however, that the usable exposure time during Coronas-F observations is severely limited by the Earth's screening and by the satellite's passage through the radiation belts at high latitudes and the South-Atlantic Anomaly.

## OBSERVATIONS

The giant flare in SGR 1806-20 was detected by Konus-Wind on December 27, 2004, in the burst mode, which was triggered by the arrival of a short soft burst that led the flare by 143 s. The record of these events in general form is pre-

sented in Fig. 1. The appearance of a “precursor” displaced the flare into the time resolution region of 0.256 s and reduced the time of its observation by half. The related losses in the volume and detail of information were largely compensated for by the operation of the Konus standby systems mentioned in the Konus-Wind section.

### The Precursor

The time history of this burst is shown in Fig. 2a. The burst emission is soft and is observed only in the G1 and G2 windows. Figure 2b presents an averaged photon spectrum of the whole burst. When it is fitted by the OTTB distribution,  $kT$  is  $36.9 \pm 0.9$  keV. In its characteristics, the precursor does not differ radically from other recurrent bursts in SGR 1806-20 while slightly standing out by its intensity.

### The Initial Pulse of the Flare

A portion of the flare time history containing the giant initial pulse is presented in Fig. 3. It was recorded by the first standby system of the instrument in the G2 and G3 windows with a time resolution of 2 ms. The flare began at  $T-T_0=142.98$  s with an avalanche-like increase in intensity that was traceable until the detector's sharp transition to a state of deep saturation at  $T-T_0=143.12$  s. The enormous intensity of the flare emission continued to keep the detector in a state of complete saturation for 0.50 s and only at  $T-T_0=143.62$  s did the final segment of the initial pulse decay become observable. Recall that when the giant flare was detected by Konus-Wind on August 27, 1998, in SGR 1900+14 and when the data obtained were analyzed, it was established that the Konus detector was deeply saturated at an incident flux of  $F_E \gtrsim 2.4 \times 10^{-2}$  erg cm $^{-2}$  s $^{-1}$  (Mazets et al. 1999a). For this flare, the saturation lasted for  $\simeq 0.2$  s. All of the main flare evolution phases, its rise, passage through the maximum, and decay, occurred in the time interval when the detector was saturated. Undoubtedly, the actual fluxes from the flare at these phases exceed the above instrumental value of  $F_E$  by many factors; the longer the saturation stage, the greater this excess. However, further direct or indirect information is required to reliably estimate the flare intensity. By a stroke of luck, such direct information was obtained for the flare in SGR 1806-20

during Coronas-F observations.

### Compton Scattering of the Initial Pulse of the Flare by the Moon

During the flare of December 27, 2004, Coronas-F was shadowed from SGR 1806-20 by the Earth. At 21:30:29.303 UT, Helicon recorded a weak short burst whose profile is shown in Fig. 4a in the trigger mode with a high time resolution of 2.048 ms. The burst lasted  $\simeq 180$  ms. In this time, two multichannel spectra were measured with an accumulation time of 65.536 ms each. The combined spectrum is shown in Fig. 4b. The shape of the spectrum is quite unusual for gamma-ray bursts. It was immediately suggested that the Compton reflection of the giant initial pulse of the flare from the Moon was observed. This suggestion was completely confirmed by examining the spatial configuration of the Earth, the Moon, and the spacecraft relative to the direction toward SGR 1806-20. At the flare time (Fig. 5), the Sun was at an angular distance of  $5^\circ 3'$  from SGR 1806-20 and the Moon was located near the apogee of its orbit. The full moon came on December 26. The angle through which the gamma-rays of the initial pulse must be scattered in order to fall on Coronas-F is  $159^\circ 5' - 159^\circ 9'$ . The calculated time delay between the arrivals of the flare at Wind and the scattered signal at Coronas-F closely agrees with the observed value of 7.69 s. Thus, the Helicon data make it possible to reliably determine the spectrum and intensity of the initial pulse of the flare from the measured spectrum of the scattered emission and to reconstruct the time history of the most intense part of the flare from the profile of the reflected signal. For this purpose, we numerically simulated the scattering of a plane gamma-ray flux in the Moon's spherical surface layer by the Monte-Carlo method using the GEANT4 software package developed at CERN (Agostinelli et al. 2003). The elemental composition of the lunar soil was taken to be the following: O – 42%, Si – 21%, Fe – 13%, Ca – 8%, Al – 7%, Mg – 6%, and the remaining elements – 3%.

The response matrix of the Moon, which describes the escape probability of a photon with energy  $E'$  scattered through angle  $\theta = 159^\circ$  normalized to a unit solid angle, was obtained over a wide range of incident photon energies  $E$ , from 20 keV to 12 MeV. Figure 6a gives an idea of the

matrix structure. The intensity of filling the  $(E', E)$  plane with the dark color is proportional to the escape probability of a photon with energy  $E'$  for an incident photon with energy  $E$ . Two regions of maximum probability can be distinguished. The dark curve

$$E' = \frac{E}{[1 + E/mc^2(1 - \cos\theta)]} \quad (1)$$

corresponds to single scattering through angle  $\theta = 159^\circ$  with a limiting value of  $E' = 264$  keV at high  $E$ . The vertical line  $E' = 511$  keV at  $E > 2mc^2$  corresponds to the escape of an annihilation photon as a result of the interaction of photon  $E$  with the production of an electron-positron pair. The diffuse field in the graph characterizes the role of multiple scattering, whose probability is high for a thick target. Figures 6b shows examples of the matrix sections by the  $E = \text{const}$  plane, which in each case represent the corresponding scattered photon energy distribution function  $f(E', E)$ .

Using the response matrix, we can calculate the Moon's reflectances in direction  $\theta$  per unit solid angle in photon number  $\epsilon_N$  and energy  $\epsilon_E$  normalized, for example, to one incident photon with energy  $E$  as a function of  $E$ . If, for clarity, we pass from the summation over the matrix elements to integration, then the expressions for the reflectances will take the following form:  $\epsilon_N(E) = \int_{E'_{min}}^{E'_{max}} f(E', E) dE'$ ,  $\epsilon_E(E) = (1/E) \int_{E'_{min}}^{E'_{max}} f(E', E) E' dE'$ . The lower limit  $E'_{min} = 20$  keV is determined by the instrumental threshold. The upper limit  $E'_{max} = 10$  MeV was chosen in the energy range where no scattered emission is observed at the sensitivity level of the instrumentation. These dependences are shown in Fig. 7.

The Moon's response matrix was then folded with the response matrix of the Helicon gamma-ray spectrometer. To take into account the lunar disk size  $\pi R_L^2$  and the attenuation of the scattered signal in its way to Coronas-F  $\propto D_C^2$ , the response matrix was renormalized to the solid angle  $\Omega = \pi R_L^2 / D_C^2$  at which the Moon is seen from the satellite. In this form, the response matrix of the Moon-Helicon system transforms the differential photon spectrum of the flare  $I(E) = A f(E)$  to the energy loss spectrum measured by the gamma-ray spectrometer,  $n_i(E')$ .

It follows from Fig. 4a that the reflected signal is weak. It is distinguished above the background in the energy range  $\simeq 25\text{--}350$  keV in the time interval  $T-T_0$  from  $\simeq -40$  to  $\simeq 140$  ms. To improve the count statistics in the multichannel spectrum, we grouped the spectrometer's channels by two and considered the sum of the two spectra accumulated in the time interval after  $T_0$  spanning 32 4.096-ms time channels in the signal profile. Since the limitations on statistics do not allow the course of the fast spectral evolution to be traced on a millisecond time scale in full, we will proceed from the assumption that the shape of the flare spectrum  $f(E)$  in this time interval  $\simeq 131$  ms is retained and only its intensity  $A$  changes. For the subsequent analysis, note that the time profile of the total signal in two windows in these 32 channels after the background subtraction contains  $363 \pm 22$  counts. The mean number of counts per channel is  $\bar{n}=11.3$  in 4 ms. To model the instrumental spectrum, we used the XSPEC v.11.3.2p code, including the derived response matrix. We tested four models of the flare spectral intensity  $I(E) = Af(E)$ : (a) a power law with an exponential cutoff, (b) Band's model, (c) a power law, and (d) blackbody radiation.

The first model yields good agreement between the model and measured spectra:  $I(E) = AE^{-\alpha} \exp(-E/E_0)$ . The values of the parameters that minimize  $\chi^2 = 10.6/12$  dof are  $A = 1.98^{+0.47}_{-0.41} \times 10^6$  photons  $\text{cm}^{-2} \text{s}^{-1} \text{keV}^{-1}$ ,  $\alpha = 0.73^{+0.47}_{-0.64}$ ,  $E_0 = 666^{+1859}_{-368}$  keV; the energy of the peak  $\nu F_\nu$  of the spectrum is  $E_p = 850^{+1259}_{-303}$  keV. The errors in the parameters correspond to a confidence probability of 90%.

Band's model proved to be of little use for testing. At the poor statistics in the hard part of the instrumental spectrum, only a rough limit  $\beta < -1.6$  can be placed on the index  $\beta$  for the high-energy power-law tail of the model fit. In this case, the parameters  $\alpha$  and  $E_0$  do not differ from the previous model, within the error limits, giving  $\chi^2 = 10.3/11$  dof.

Formally, the power-law fit ( $\gamma = -1.4 \pm 0.1$ ,  $\chi^2 = 18.4/13$  dof) can be accepted, but it systematically overestimates the soft part of the spectrum.

The assumption about blackbody radiation yields the worst result,  $\chi^2 = 27.4/13$  dof,  $kT=116$  keV,

and may be rejected.

The model fits for cases (a) and (d) are shown in Fig. 8.

The corresponding segment of the time history of the giant flare that was completely lost on Konus-Wind when the detector was saturated can be reconstructed from the time profile of the reflected signal.

As we have noted above, the average spectral intensity of the flare determined when the spectrum of the reflected signal was fitted,  $I(E) = Af(E)$  photons  $\text{cm}^{-2} \text{s}^{-1} \text{keV}^{-1}$ , corresponds to the mean number of counts  $\bar{n}=11.3$  in any time channel of the profile  $\Delta t = 4.096$  ms. The intensity  $I_i(E) = (n_i/\bar{n})Af(E)$  photons  $\text{cm}^{-2} \text{s}^{-1} \text{keV}^{-1}$ , will then correspond to the number of counts  $n_i$  recorded in channel  $\Delta t_i$  in this segment of the profile. We can also easily calculate the integrated photon flux in interval  $\Delta t_i$ ,  $N_i(> E_i) = \int_E I_i(E)dE$ , and the integrated energy flux  $F_i(> E_i) = \int_E EI_i(E)dE$ ; the integration range extends from the sensitivity threshold of the instrumentation  $E_1 \simeq 20$  keV to the energy  $E_2 \simeq 5$  MeV above which the contribution to the integral is negligible.

When reconstructing the time history of the initial pulse, particularly its leading edge, we must take into account another significant factor. When the flare is scattered by a spherical Moon, the profile of the reflected signal is smeared. The plane flux from the flare  $N(t)$  reaches different areas of the lunar surface at different times. Accordingly, the scattered photons come to a remote observer with different delays. For backscattering, the maximum difference in the relative delay is  $\Delta\tau_{max} = 2R_L/c = 11.6$  ms, where  $R_L$  is the lunar radius and  $c$  is the speed of light. The relationship between the smeared profile of the signal reflected from the Moon,  $N_{refl}(t)$ , and the flux from the flare incident on it,  $N(t)$ , can be derived from simple geometrical considerations:

$$N_{refl}(t) = k \int_0^2 N(t - \tau)(1 - \tau/2)d\tau \quad (2)$$

Here, the time  $t$  and the delay  $\tau$  are measured in units of  $R_L/c$ . The coefficient  $k$ , which takes into account the attenuation during scattering, is unimportant for the problem under consideration and can formally be set equal to one.

This integral equation at the poor  $N_{refl}(t)$  statistics can hardly be effectively used to correct the entire profile  $N(t)$ . However, the equation is very useful for estimating the width of the leading edge of the flare. Our calculations indicate that the actual width of the leading edge of the flare in the reflected signal increases by  $\leq 2R_L/c = 11.6$  ms. Figure 9 shows the segment of the time history of the initial pulse reconstructed from Helicon observations in the interval  $\Delta T=180$  ms. The fluence in it is  $S = 0.87^{+0.50}_{-0.24}$  erg cm $^{-2}$  at a confidence level of 90%. Outside this interval, the assumption that the average shape of the spectrum  $f(E)$  is retained is no longer applicable. On the contrary, the G2/G1 hardness variation shown in Fig. 4 indicates that the flare spectrum rapidly becomes increasingly soft. Note that such a situation took place in the August 27, 1998 flare from SGR 1900+14 (Mazets et al. 1999a). The fluence in the decaying tail of the pulse does not exceed a few percent of the fluence in the interval  $\Delta T=180$  ms. Thus, the estimate of  $S = 0.87^{+0.50}_{-0.24}$  erg cm $^{-2}$  characterizes the fluence of the entire pulse, within the error limits.

## THE PULSATING TAIL OF THE FLARE

The Konus-Wind record of the pulsating tail of the flare in three energy windows (G1, G2, and G3) is shown in Fig. 10. Also shown is the time variation of the hardness ratio G2/G1. The count rate in the G3 window is low, but it exceeds the background level statistically significantly. After  $T-T_0=230$  s, the record of the flare ended, giving way to data output to onboard memory. The count rate in the G2 window recorded with a resolution of 3.68 s by the second standby system of the instrument gives a general idea of the duration and intensity of the flare tail. The accumulation time, 3.68 s, is close to half the pulsation period, 7.56 s, which leads to the pattern of deep beats. Therefore, a record with a resolution of 7.36 s is shown in Fig. 11.

The energy spectra in the flare tail in the segment of transition from the main peak to the steady-state pattern of pulsations until  $T-T_0=152$  s was measured with an accumulation time of 0.256 s. Subsequently, at the final stage of the trigger mode of measurements, the accumulation time was 8.192 s.

The soft part of the photon spectra, just as the spectra of recurrent bursts, is well fitted by a distribution close to OTTB radiation. Figure 12 shows the time history of the initial part of the pulsating tail in the G1 and G2 windows and gives the spectral parameters  $kT$  for 30 spectra measured with an accumulation time of 0.256 s. We see that  $kT$  correlates with the radiation intensity.

The hard part of the pulsation spectra exhibits a significant feature that was not noticed previously in two other flares: at energy  $\simeq 200$  keV, the exponential cutoff with  $kT \simeq 30$  transforms into a hard power-law tail that extends with an index  $\gamma \simeq -1.7$  to energy  $\sim 10$  MeV. The intensity of the emission in the tail is low and can be detected with an acceptable statistical accuracy by adding up several successive spectra. As an example, Fig. 13 presents several such spectra. The time variation of the energy flux in the power-law tail at energies 0.5–8 MeV is shown in Fig. 14. Unfortunately, the data obtained do not allow the question of whether the intensity of the power-law tail is modulated with a period of 7.56 s to be clarified due to the long accumulation time of the spectra.

Under the assumption that the shape of the average spectrum shown in Fig. 13d does not change significantly throughout the decaying tail of the flare (Fig. 10), the fluence in it is  $S_{tail} \simeq 8 \times 10^{-3}$  erg cm $^{-2}$ .

## THE SGR AFTERGLOW

Yet another feature in the behavior of SGR 1806-20 was observed after the flare. Mereghetti et al. (2005) reported that the SPI-ACS system onboard the INTEGRAL satellite observed the appearance and decay a hard afterglow from SGR 1806-20 with a fluence comparable to the fluence in the flare tail in the interval from  $\sim 400$  to  $\sim 4000$  s after the onset of the giant flare.

The Konus-Wind measurements in the background mode were resumed after the flare data were rewritten to memory 5075 s after  $T_0$ . Nevertheless, we analyzed the background measurements a day before and after the flare; the results are presented in Fig. 15. Generally, the background variations in the hard G2 and G3 windows are determined by the flux variations of cosmic ray, mostly of a solar origin. The Z ( $E > 10$  MeV) window serves to monitor the cosmic-ray flux. No

data in the soft G1 window were used, since unpredictable variations in the flux from X-ray sources manifest themselves in it.

Note that SGR 1806-20 lies near the ecliptic and the two Konus-Wind detectors, S1 and S2, are irradiated by the source identically. The observed small differences in the count rates are related to the actual boundaries of the energy windows.

We see from Fig. 15a that the background variation in the G2 and G3 windows of both detectors generally follows the background in the Z window. However, immediately after the interruption of the measurements to rewrite the data, excess emission without any signatures in Z was observed in the G2 and G3 windows. This picture is consistent with the assumption that the source of hard X-ray and gamma-ray emission began to act during the interruption of the measurements and was located near the ecliptic. We may conclude that the decaying phase of the SGR afterglow detected on INTEGRAL is observed. The data from the two detectors were added and the results are presented in Fig. 15b. The afterglow is traceable until  $T-T_0 \sim 12000$  s. The ratio of the sums of the counts in the G3 and G2 windows is  $0.385 \pm 0.055$ . For a power-law spectrum, this hardness ratio corresponds to an index of  $\sim -1.6$ . The fluence in the observed phase of the afterglow in the energy range 80–750 keV is estimated to be  $\sim 2 \times 10^{-4}$  erg  $\text{cm}^{-2}$ .

## THE SGR ACTIVITY BEFORE AND AFTER THE FLARE

The emission of recurrent bursts from SGR 1806-20, just as from other gamma repeaters, is distributed very nonuniformly in time. SGR 1806-20 was detected and localized in the period of high activity in the early 1980s (Atteia et al. 1987; Laros et al. 1987). The source was also highly active in 1996. From January to May 2004, Konus-Wind observed a total of two bursts in the trigger mode. However, a new period of high activity began in May and Konus and Helicon recorded 74 trigger bursts before the giant flare. After the flare until the end of 2005, 22 events were observed. These data were plotted in the  $S$ - $\Delta T$  diagram (Fig. 16). The 2005 events are slightly less intense (by a factor of 2–3). The precursor, a short burst appeared 142 s before the flare, is also

presented in the diagram. It is strongest in energetics, but it should hardly be considered as an event that differs radically from the entire set. In our opinion (Golenetskii et al. 2004), the appearance of close groups or series of a larger number of recurrent bursts filling a time interval of several minutes is considerably stronger evidence for the preflare state of the source. Three such series were observed in SGR 1806-20: on October 5, 2004 (83 days before the flare), December 21, 2004 (6 days before the flare), and December 25, 2004 (2 days before the flare). It is important to mention that a similar series of recurrent bursts was observed on May 30, 1998, in SGR 1900+14 89 days before the giant flare of August 27, 1998 (Aptekar et al. 2001). Note also that the Sun was highly active in the summer of 1998. For many hours and days, the background level attributable to intense solar cosmic-ray fluxes often increased to a level that ruled out the trigger recording of both single short bursts and, possibly, a new series.

All four series are presented in Fig. 17 in the record with a time resolution of 0.256 s. The total fluence of each series  $S$  is given in the caption to the figure.

## DISCUSSION

The time history of the activity of SGR 1806-20 in 2004 considered here, whose culmination was the giant flare on December 27, 2004, can be divided into a series of characteristic stages.

- (1) The source's reactivation accompanied by an enhanced emission rate of recurrent bursts with cases of their close grouping into short series of several tens of events.
- (2) The emission of a giant initial pulse of the flare with a hard, rapidly evolving spectrum.
- (3) The stage of transition from the initial pulse to the pulsating tail of the flare.
- (4) The decaying soft pulsating tail of the flare.
- (5) The prolonged hard afterglow of the source.
- (6) The gradual decay of the emission of recurrent bursts among which separate longer-duration events appear.

Such a sequence of events, at minimum deviations from it, was mainly also characteristic of the development of activity in SGR 1900+14 in 1998 with the giant flare on August 27, 1998 (Mazets et al. 1999a). In both cases, the observations were performed with the same Konus-Wind instrument. However, late in August, the solar activity was high and the solar cosmic-ray fluxes led to a manifold increase in the radiation background level. The high background prevented the detection of such weak effects as the remote afterglow of the source or the hard powerlaw tails in the pulsation spectrum. For this reason, the question of whether these exist for the flare in SGR 1900+14 is still an open question.

The giant flare of March 5, 1979, in SGR 0526-66 and the subsequent emission of recurrent bursts until the middle of 1983 were observed on Venera space stations with the Konus instrumentation (Aptekar et al. 2001). This instrumentation was appreciably inferior in sensitivity and, particularly, information content to the Konus-Wind instrumentation. Nevertheless, it can be assumed with a fair degree of confidence that SGR 0526-66 was in quiescence before the flare of March 5, 1979, in half a year of observations. Note that this gamma repeater, having emitted  $\simeq 20$  recurrent bursts, has remained quiescent for more than 20 years.

Thus, we may conclude that, despite the close similarity between the giant flares in the three SGRs, the individual differences in their activity before and after the flare show up quite clearly. Moreover, the universality of the picture of the giant flare itself in SGR is violated by the very intense flare of June 18, 1998, in SGR 1627-41 (Mazets et al. 1999b). The flare was several thousand times more intense than the recurrent bursts in this gamma repeater. This flare lasted  $\simeq 0.5$  s, but it was abruptly cut off, without leaving even the slightest trace of the decaying tail.

### The Picture of Pulsations

It is of interest to compare the pulsations in the three flares. Their profiles averaged over several periods to smooth out small fluctuations are shown in Fig. 18. Each profile consists of several (from two to four) overlapping peaks. In all three cases, the maximum modulation depth is approximately the same,  $\simeq 85\%$ .

The flare tail is widely believed to be emitted by a cloud of dense relativistic electron-positron plasma with an admixture of baryons trapped and confined by the superstrong magnetic field of a neutron star when the fireball with which the giant initial pulse of the flare is associated is ejected from it. The ultimate configuration of the trapped part of the fireball is formed during the transition from a short initial pulse to a uniform repetitive picture of pulsations. The rigid fixing of the magnetic trap's field lines in the neutron star's highly conductive crust ensures the subsequent stability of the formed cloud configuration.

In our opinion, the crucial role in forming the observed picture of deep modulation of the slowly decaying flare tail emission belongs to the shape of the angular beam and to its changing (due to the rotation of the neutron star) orientation relative to the observer's position on the celestial sphere. In the inertial equatorial coordinate system associated with the neutron star, the observer's position is specified by right ascension  $\alpha_{obs}$  and declination  $\delta_{obs}$ . For the emission to be recorded as a separate peak, it must have a beam that crosses the observer's celestial parallel, a small circle with  $\delta = \delta_{obs}$ , and, hence, must pass through the observer's direction as the star rotates. In this case, the observed shape of the peak will be determined by the shape of the angular beam in its section by the  $\delta_{obs}$  parallel. The angular beam FWHM in this section  $\Delta\theta$  is related to the apparent FWHM of the peak in the star's rotation phase  $\Delta\phi$  by  $\Delta\theta = 2\pi\Delta\phi \cos \delta_{obs}$ . When considering the shape of the peak recorded in different energy windows (see, e.g., Fig. 10), we can establish that the beam width along the declination circle decreases with increasing energy. The overall variation in hardness G2/G1 and its peculiarities in the region of overlap between the neighboring pulsation peaks can be attributed precisely to this circumstance.

However, when the structure of the pulsations with several peaks is considered, the difficult question of the number of emission sources on the neutron star, including the sources invisible to the observer, arises.

The assumption about the distribution of trapped plasma in large number of magnetic traps would be an undesirable complication of the flare tail emission model. The situation becomes slightly less acute if we assume that the



angular beam is close to a fan pattern, having the shape of a widely opened hollow cone. At each given time, such a beam will be projected onto the celestial sphere in the form of a long stripe elongated along a celestial circle of a large angular radius inclined to the stellar equator. Such a stripe can cross the observer's parallel  $\delta_{obs}$  twice and two pulsations peaks will be observed in one rotation of the neutron star, as in SGR 0526-66. If no additional, more peculiar assumptions about the complex spatial shape of the beam is invoked, then the presence of two fan beams will be required to explain the pattern of pulsations in SGR 1900+14 and SGR 1806-20. The reasoning behind the formation mechanism of two fan beams given ad hoc for the flare of August 27, 1998, (Thompson & Duncan 2001) does not look quite convincing, but it undoubtedly serves as the first evidence for the existence of yet another problem requiring its solution. To explain the peculiarities of the giant flare in SGR 1627-41, we can assume that, in this case, the direction of the neutron star's rotation axis makes a small angle with the observer's line of sight. The flare occurred in the stellar hemisphere invisible to the observer. The magnetic trap with trapped plasma remains invisible at all rotation phases of the star and the possibility of detecting the flare tail is completely ruled out.

### The Energetics of SGR 1806-20

The fluence of the initial pulse of the flare at energies  $E > 16.5$  keV in the time interval after the flare onset  $\Delta T = 0.6$  s is  $S = 0.87^{+0.50}_{-0.24}$  erg cm<sup>-2</sup>. The peak flux of the flare in a time interval of 4 ms is  $F_{peak} = 13.1^{+8.0}_{-4.4}$  erg cm<sup>-2</sup> s<sup>-1</sup>. The fluence in the transition region and the pulsating tail of the flare before its decay is  $S_{tail} \simeq 8 \times 10^{-3}$  erg cm<sup>-2</sup>. The flux at the main pulsation peak for the first rotations of the star is  $F \simeq 4.9 \times 10^{-5}$  erg cm<sup>-2</sup> s<sup>-1</sup> (in 0.256 s). The intensity of recurrent bursts varies over a wide range, from  $\sim 2 \times 10^{-7}$  to  $\sim 2 \times 10^{-4}$  erg cm<sup>-2</sup> at a duration of  $\sim 0.1$ –20 s (Fig. 16).

The estimates of the distance  $D$  to SGR 1806-20 are being discussed (see, e.g., Cameron et al. (2005); McClure-Griffiths & Gaensler (2005)). We take the widely used value of  $D = 15$  kpc. We also assume that the emission of the initial pulse is isotropic in a solid angle of  $4\pi$  sr. Our esti-

mates of the energy output and peak luminosity of the initial pulse, tail, and recurrent bursts are summarized in the Table 1.

For the afterglow, we estimated the energy release only in its final stage. According to Mereghetti et al. (2005), the total energy of the afterglow is comparable to the energy emitted in the flare tail.

This work was supported by the Federal Space Agency of Russia and the Russian Foundation for Basic Research (project no. 06-02-16070).

### REFERENCES

- Agostinelli, S., et al. 2003, NIM A, 506, 250
- Aptekar, R. L., et al. 1995, Space Sci. Rev., 71, 265
- Aptekar, R. L., et al. 2001, ApJS, 137, 227
- Atteia, J. L., et al. 1987, Soviet Astronomy Letters, 13, 416
- Borkowski, J., et al. 2004, GCN Circ. 2920
- Cameron, P. B., et al. 2005, Nature, 434, 1112
- Cline, T., et al. 2000, ApJ, 531, 407
- Feroci, M., et al. 1999, ApJ, 515, L9
- Golentskii, S., Ilinskii, V., & Mazets, E. 1984, Nature, 307, 41
- Golenetskii, S., et al. 2004, GCN Circ. 2769
- Hurley, K., et al. 1999, Nature, 397, 41
- Hurley, K., et al. 2004, GCN Circ. 2921
- Hurley, K., et al. 2005, Nature, 434, 1098
- Laros, J. G., et al. 1987, ApJ, 320, L111
- Mazets, E. P., et al. 1979a, Nature, 282, 587
- Mazets, E. P., Golenetskii, S. V., & Gur'yan, Yu. A. 1979b, Soviet Astronomy Letters, 5, 343
- Mazets, E. P., et al. 1999a, Astronomy Letters, 25, 635
- Mazets, E. P., et al. 1999b, ApJ, 519, L151
- Mazets, E., et al. 2004, GCN Circ. 2922

McClure-Griffiths, N. M., & Gaensler, B. M. 2005, ApJ, 630, L161

Mereghetti, S., et al. 2005, ApJ, 624, L105

Oraevskii, V. N., et al. 2002, Physics-Uspehi, 45, 886

Palmer, D. M., et al. 2005, Nature, 434, 1107

Smith, E., et al. 2005, GCN Circ. 2927

Terasawa, T., et al. 2005, Nature, 434, 1110

Thompson, C., & Duncan, R. C. 1995, MNRAS, 275, 255

Thompson, C., & Duncan, R. C. 1996, ApJ, 473, 322

Thompson, C., & Duncan, R. C. 2001, ApJ, 561, 980

Woods, P., et al., 1999, ApJ, 519, L139

Woods, P. M., et al. 2005, GCN Circ. 2950

*Translated by V. Astakhov*

TABLE 1  
ENERGETICS OF SGR 1806-20

	$Q_{rad}, \text{ erg}$	$L_{max}, \text{ erg s}^{-1}$
Initial pulse	$\simeq 2.3 \times 10^{46}$	$\simeq 3.5 \times 10^{47}$
Pulsating tail	$\simeq 2.1 \times 10^{44}$	$\simeq 1.3 \times 10^{42}$
Recurrent bursts	$5 \times 10^{39} - 5 \times 10^{42}$	$2 \times 10^{41} - 2 \times 10^{42}$

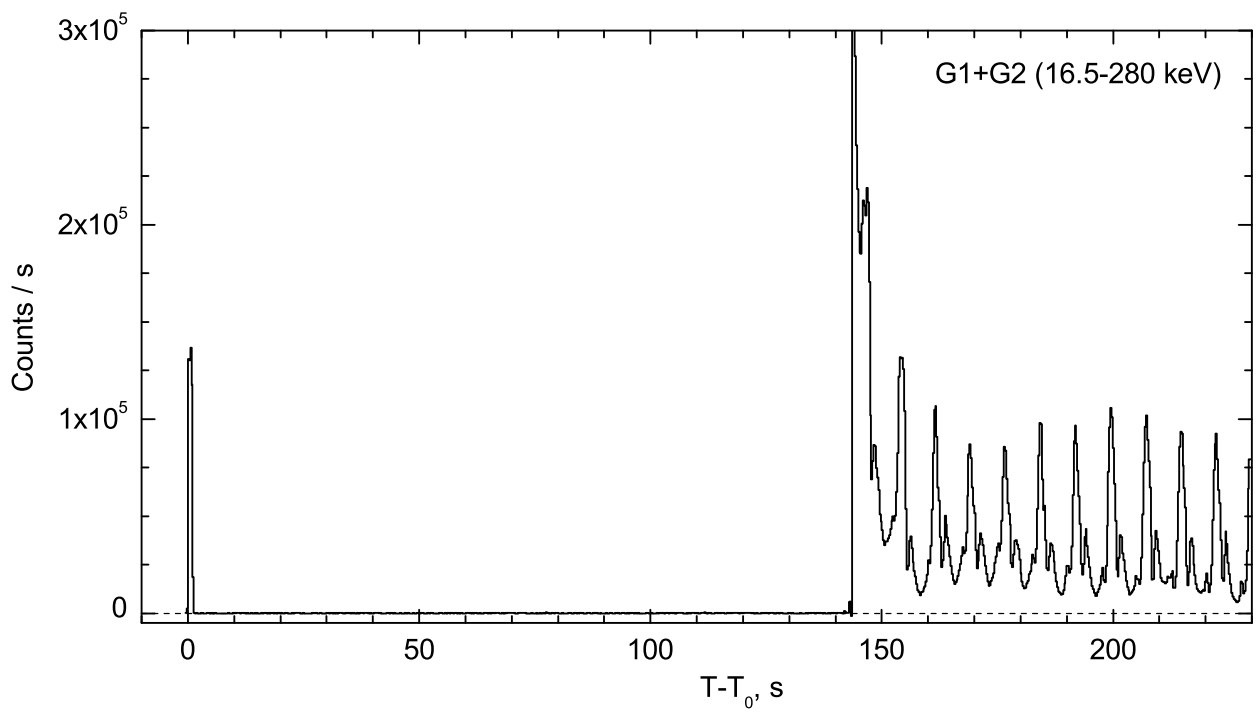


Fig. 1.— Trigger record of the December 27, 2004 flare for the sum of the G1 and G2 windows with a time resolution of 0.256 s.

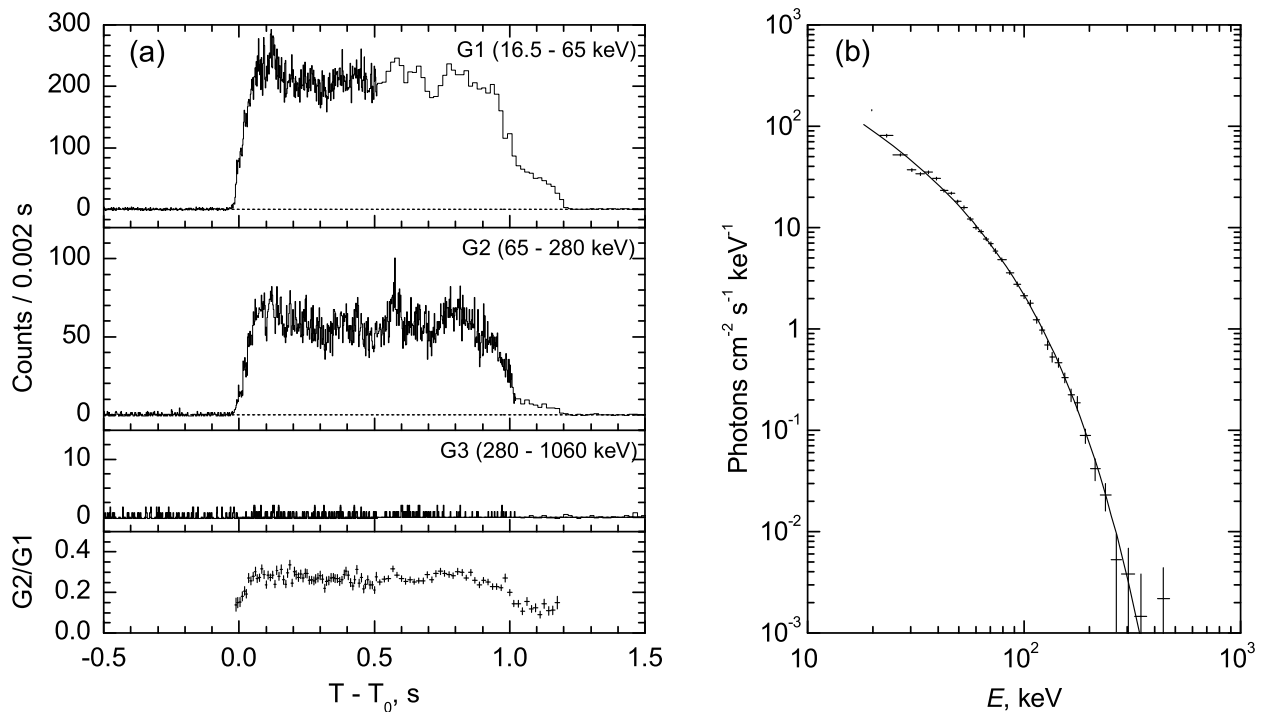


Fig. 2.— Precursor of the giant flare. (a) The time history in three energy windows recorded by the Konus-Wind detector at  $T_0=21:27:59.447$  UT (the background was subtracted). In the G2 and G3 windows, the resolution is 2 and 16 ms before and after 1 s, respectively; in the G1 window, the resolution is 2 and 16 ms before and after 0.512 s, respectively. (b) The spectrum measured in  $T-T_0=0-1.024$  s.

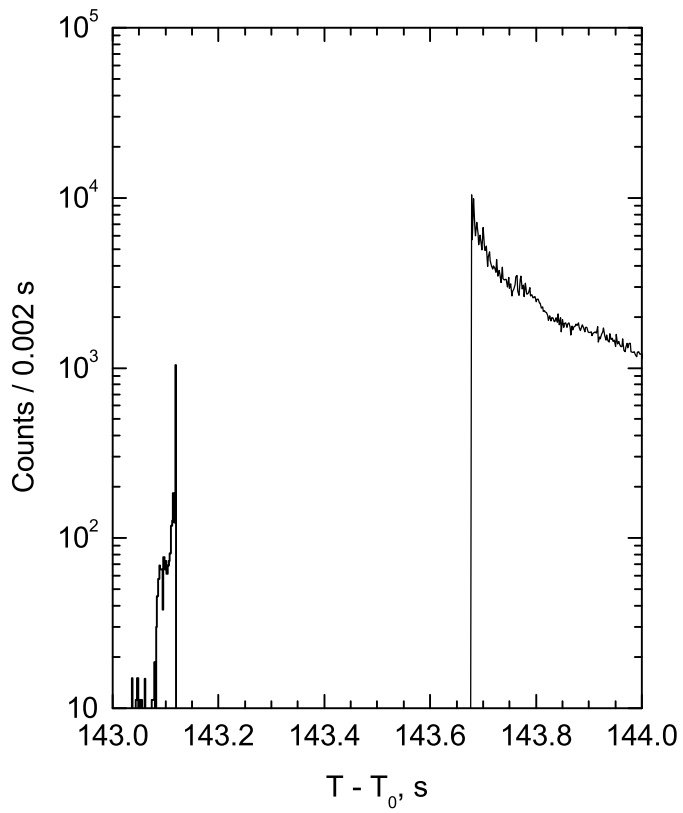


Fig. 3.— Initial pulse of the giant flare (the sum of windows G2+G3). The sharp boundaries of the state of complete saturation are indicative of an enormous rate of change in emission intensity at the leading edge and decay of the flare.

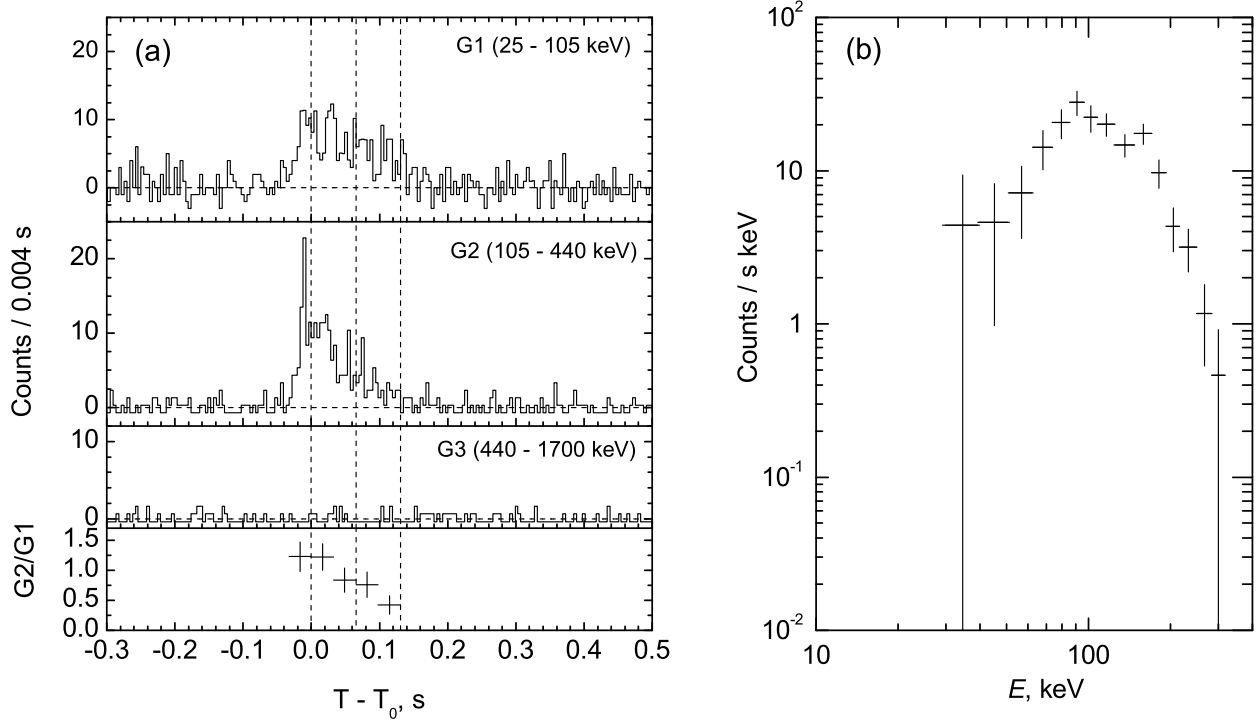


Fig. 4.— (a) Helicon time history of the initial pulse of the giant flare on December 27, 2004, reflected from the Moon.  $T_0=21:30:29.303$  UT, the time resolution is 4 ms, the background was subtracted. The hardness ( $G2/G1$ ) variation points to rapid spectral evolution of the emission. The vertical lines mark two measurement intervals of multichannel spectra. (b) The combined spectrum for the two intervals.

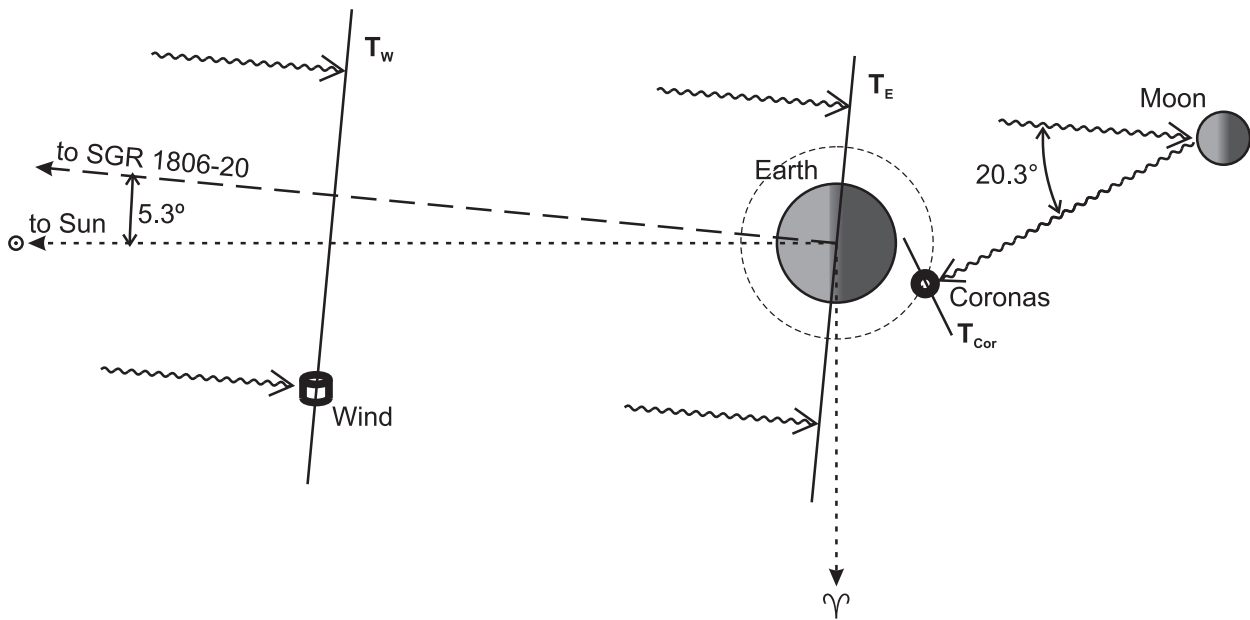


Fig. 5.— Scheme illustrating the Konus-Wind and Helicon-Coronas-F observations of the giant flare. The leading edge of the flare from SGR 1806-20 arrives at Wind at time  $T_W$ , passes by the Earth at  $T_E = T_W + 5.086$  s, reaches the Moon and is reflected from it, and, finally, the reflected emission reaches the Helicon-Coronas-F detector at  $T_{Cor} = T_W + 7.69$  s.



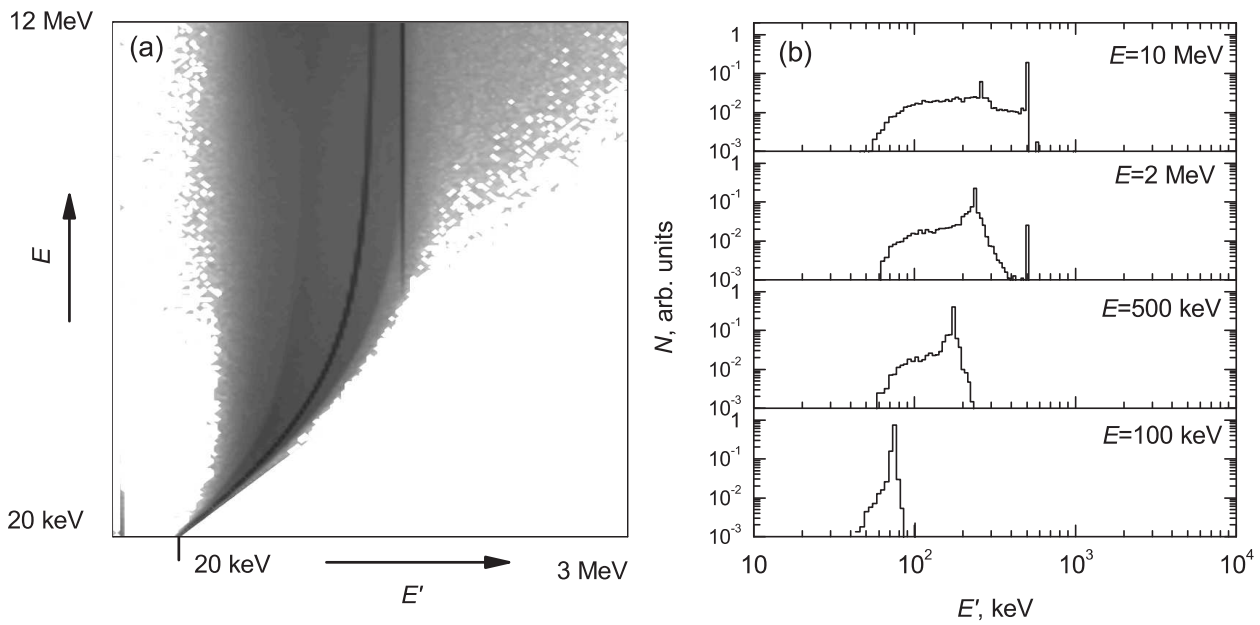


Fig. 6.— Response matrix of the Moon calculated for an angle of reflection of  $159^\circ$ . (a) The quasi-three-dimensional distribution of escaped photons for various energies  $E$  of incident  $\gamma$ -ray photons: the darker color corresponds to a higher escape probability of a photon with given energy  $E'$ . The two dark lines are the curve corresponding to single Compton scattering and the straight line characterizing the escape of annihilation 0.511-MeV photons due to the production of pairs by hard flare photons. (b) The energy distribution of escaped photons for several  $E$ .

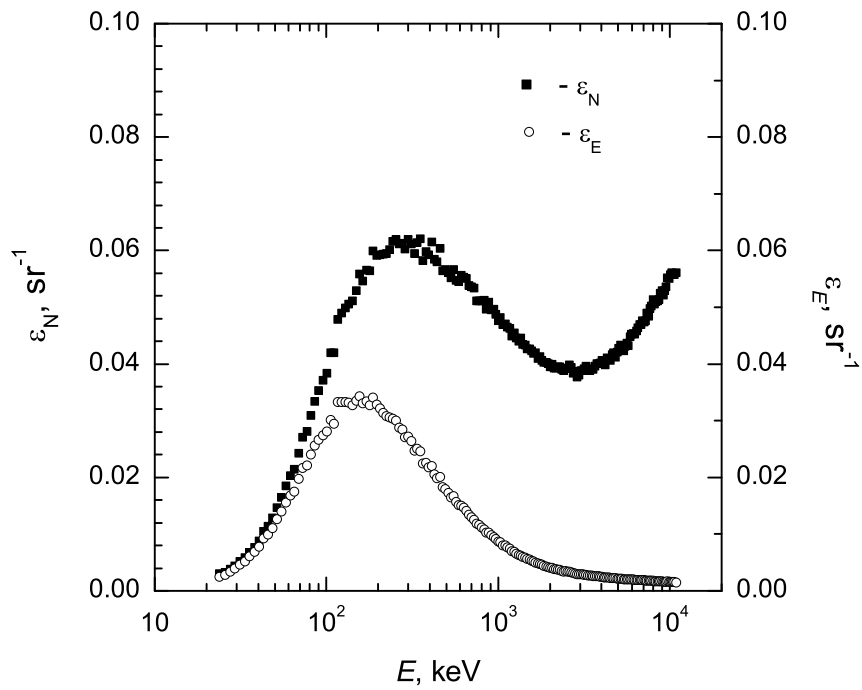


Fig. 7.— Efficiency of the reflection of  $\gamma$ -ray emission by the Moon in photon number  $\epsilon_N$  and energy  $\epsilon_E$ : respectively, the number and energy carried away by the photons escaped at angle  $\theta = 159^\circ$  per unit solid angle  $\Omega$  as a function of  $E$ .

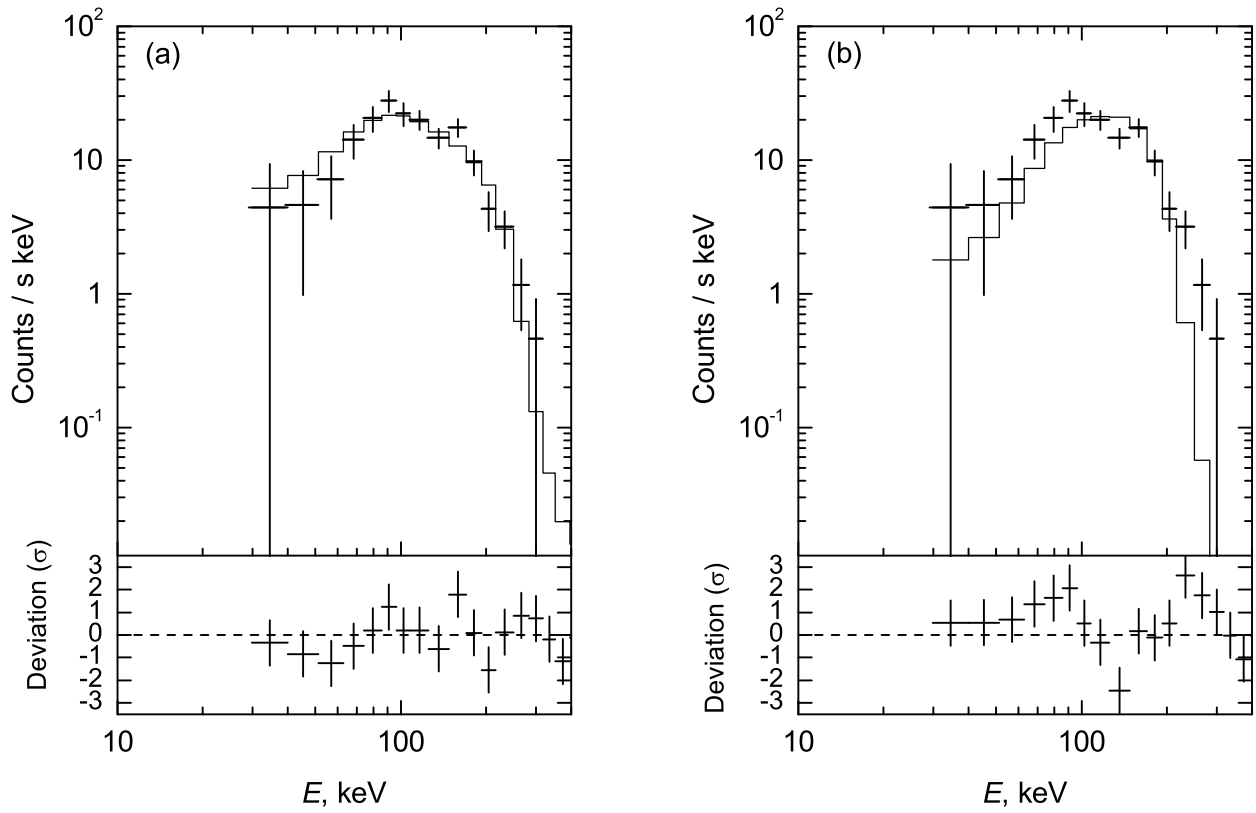


Fig. 8.— Combined spectrum of the reflected initial pulse of the giant flare recorded by the Helicon detector (accumulation time 0.131 s). The solid step lines indicate the various spectral model fits. (a) A power law with an exponential cutoff,  $\chi^2=10.6/12$  dof; (b) a blackbody model,  $\chi^2=27.4/13$  dof.

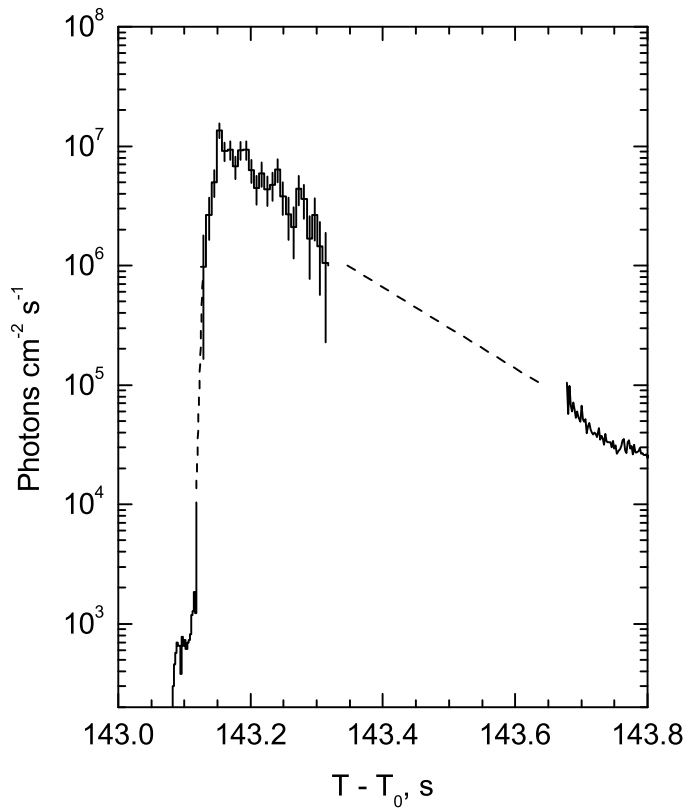


Fig. 9.— Reconstructed time history of the initial pulse of the giant flare. The upper part of the graph was reconstructed from Helicon data ( $1\sigma$  statistical errors are shown) and the lower part was reconstructed from Konus-Wind data. The dashed lines denote the intervals in which the emission is intense enough to saturate the Konus-Wind detector, but is not intense enough for the reflected signal to be recorded by Helicon.

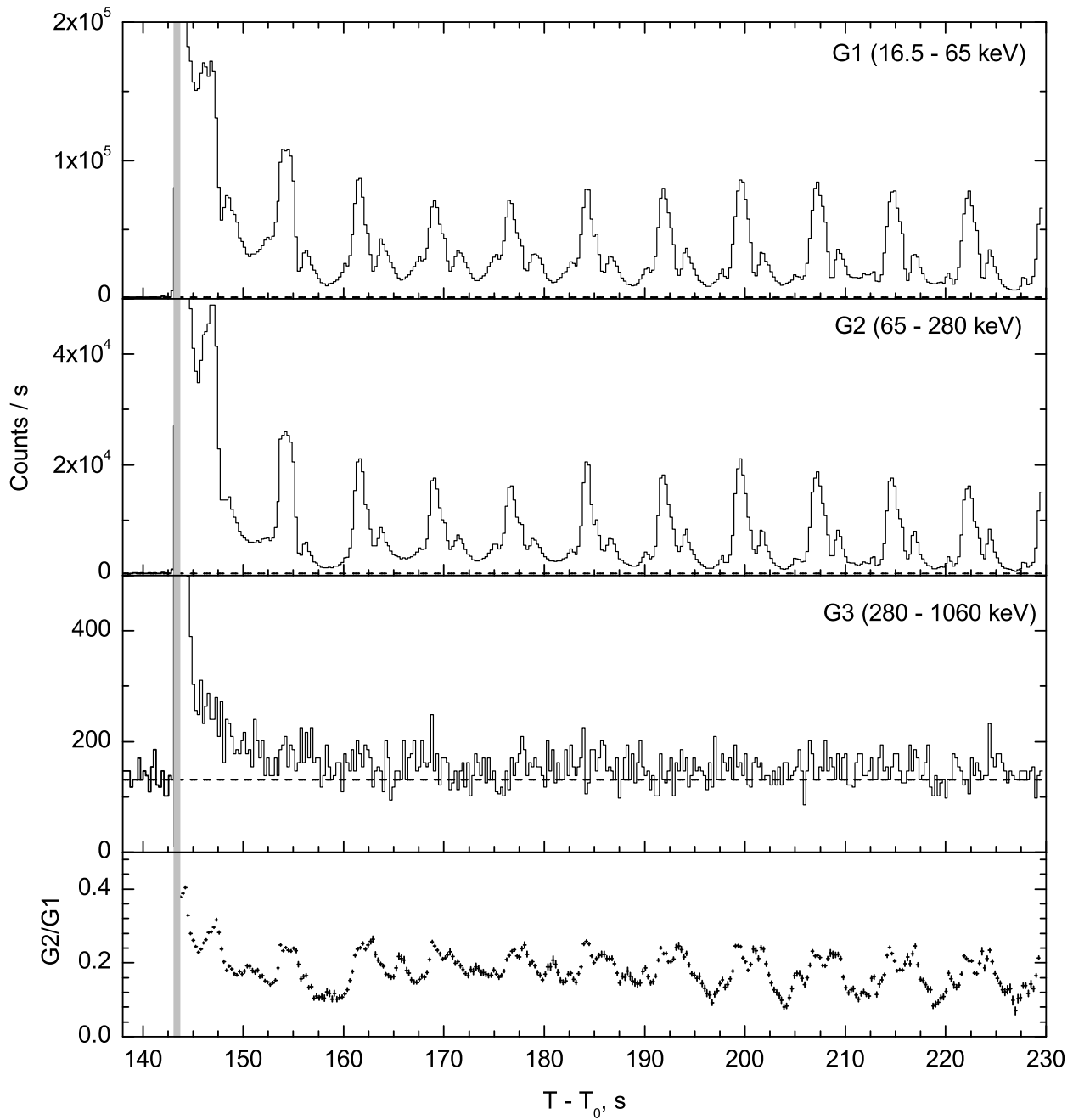


Fig. 10.— Time history of the giant flare on December 27, 2004, recorded by the Konus-Wind detector,  $T_0=21:27:59.447$  UT. The trigger part of the time history in three windows: G1(16.5–65 keV), G2(65–280 keV), and G3(280–1060 keV), and the hardness ratio G2/G1. The vertical gray line marks the time interval when the detector was in a state of complete saturation.

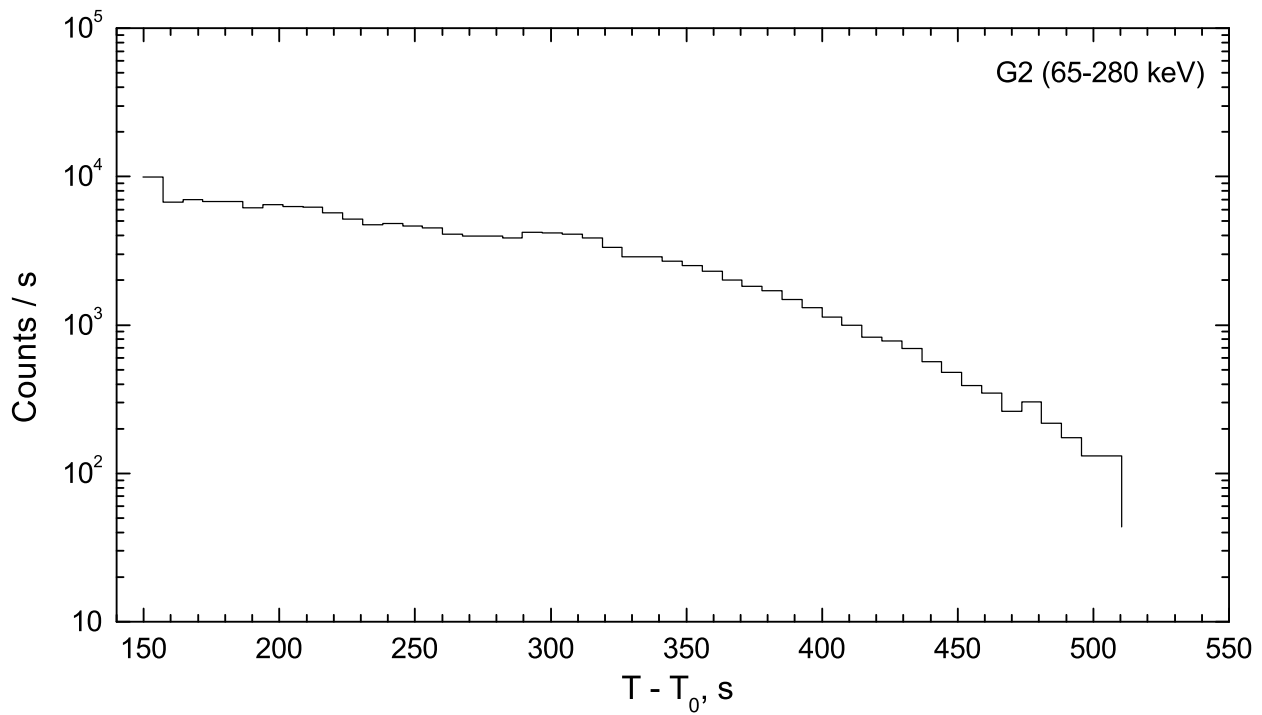


Fig. 11.— Time history of the tail of the giant flare on December 27, 2004, in the G2 window with a resolution of 7.36 s. Konus-Wind data,  $T_0=21:27:59.447$  UT. The tail rapidly decays after  $T-T_0=500$  s.

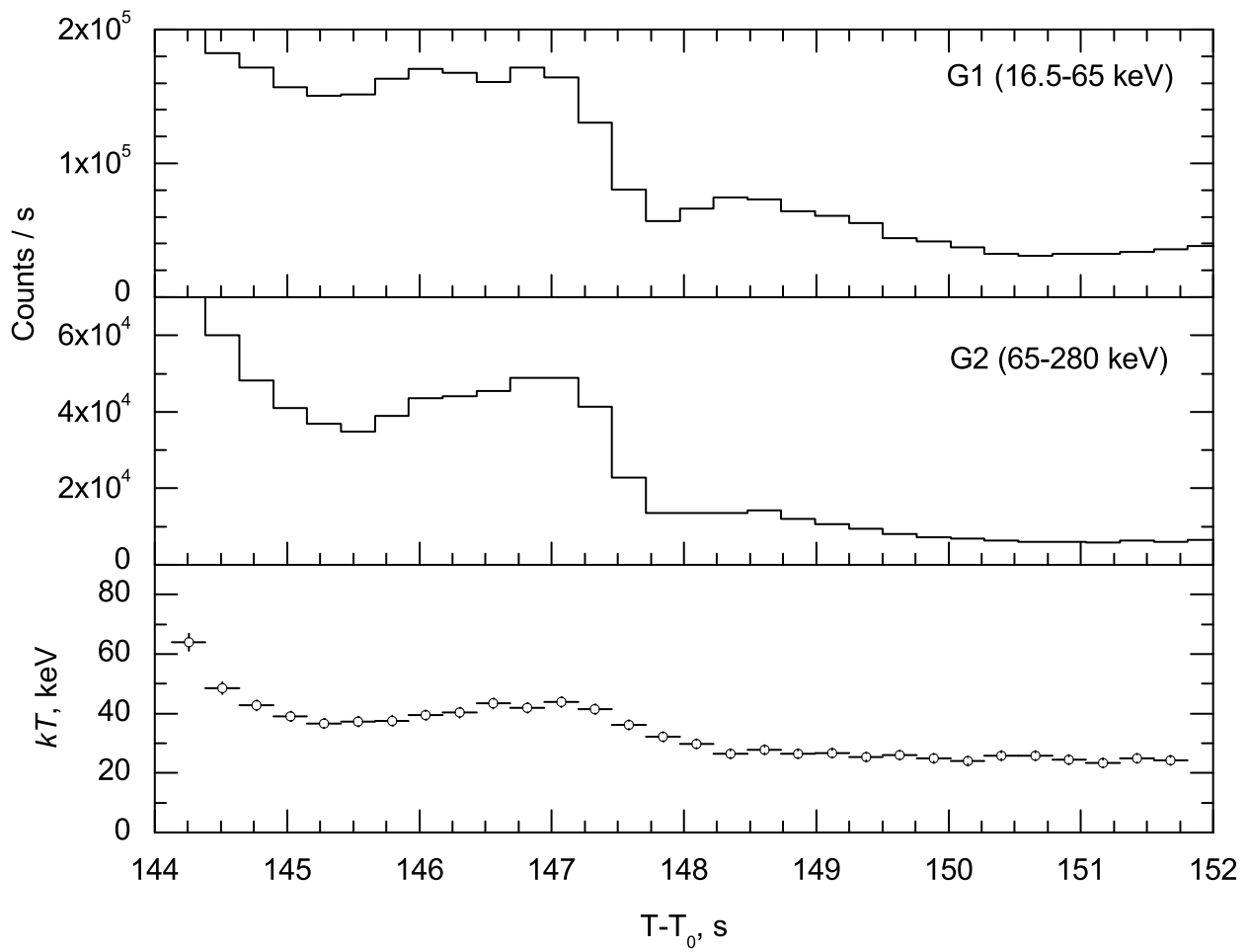


Fig. 12.— Initial part of the tail of the giant flare on December 27, 2004.

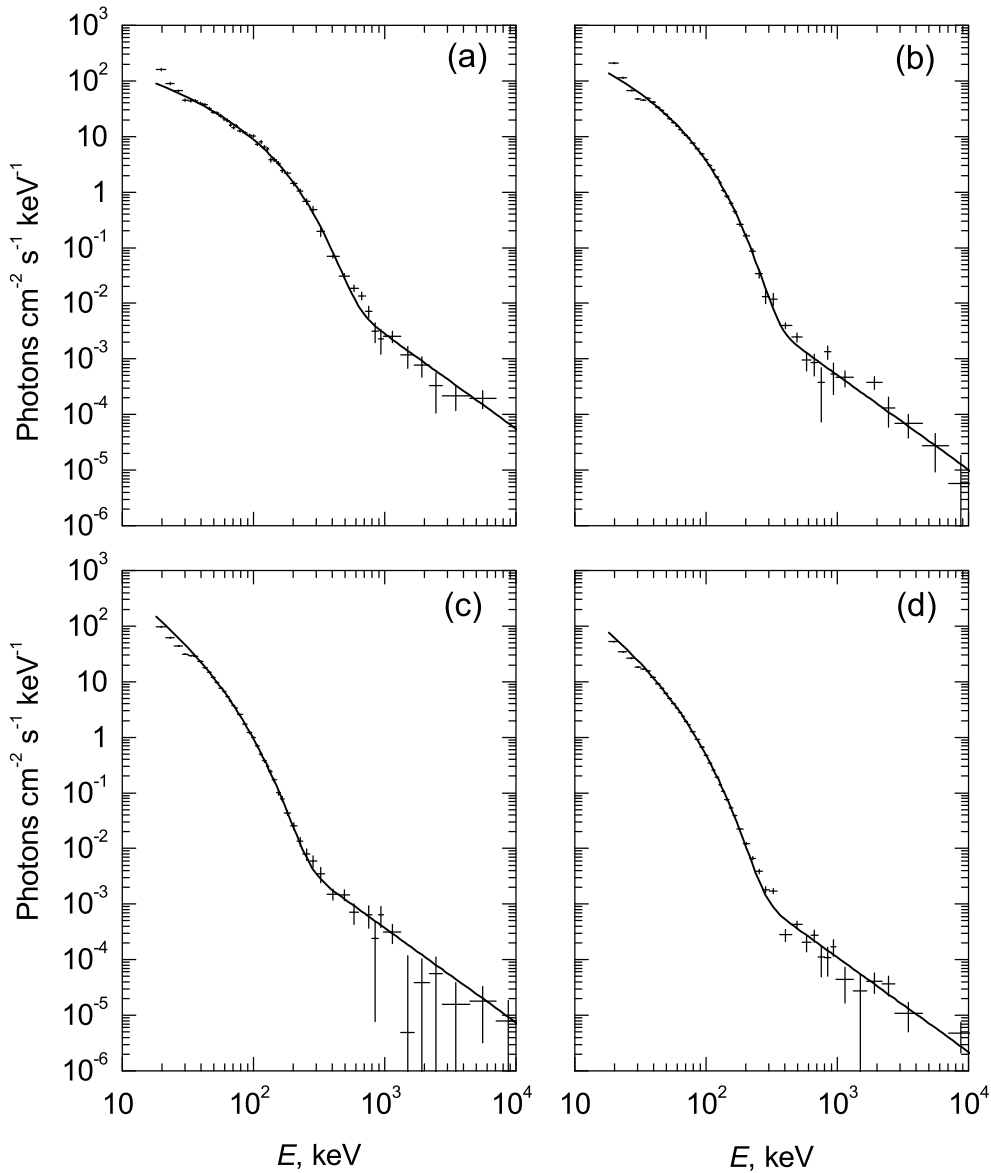


Fig. 13.— Spectra of the pulsating tail measured by the Konus-Wind detector. All spectra consist of two components: a low-energy component similar to the spectra of recurrent bursts with  $kT \simeq 30$  keV and a hard power-law component with an index  $\gamma \simeq -1.7$ . For each spectrum, this two-component model is indicated by the solid line. The spectra were measured in the following intervals: (a) 0.872–1.384 s, (b) 1.384–4.456 s, (c) 4.456–8.808 s, and (d) 8.808–74.344 s (the time is measured from the onset of the giant flare,  $T-T_0=142.98$  s).



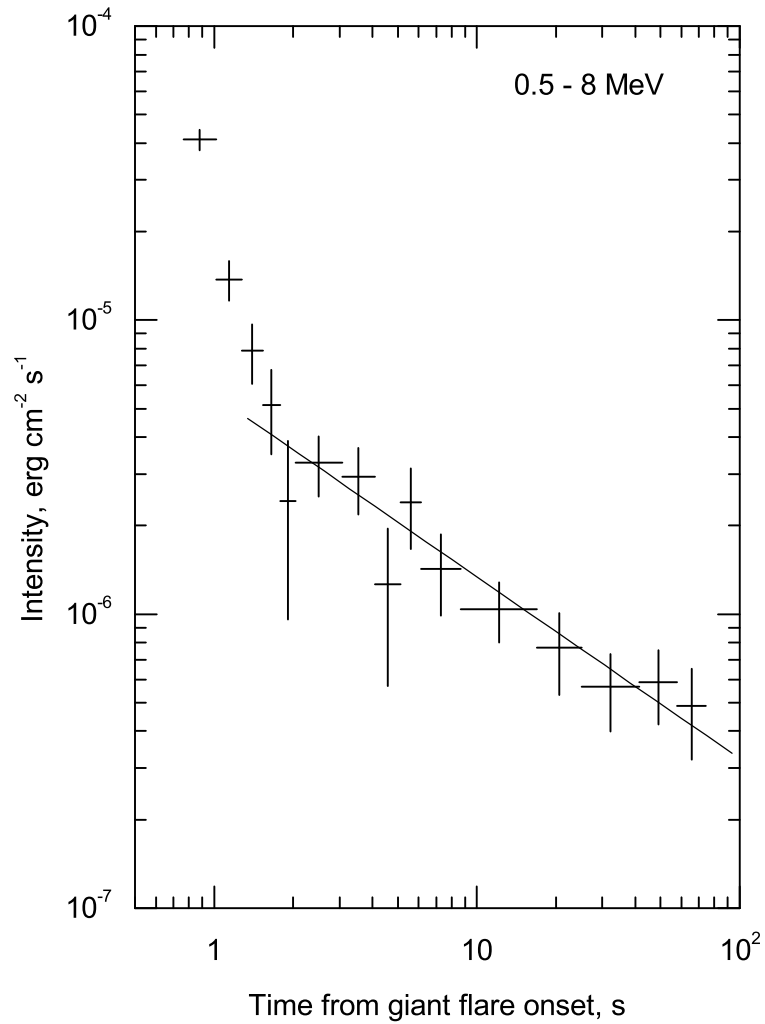


Fig. 14.— Intensity of the hard (0.5–8 MeV) component vs. time (the time is measured from the onset of the giant flare,  $T-T_0=142.98$  s). The solid line indicates the dependence  $\propto t^{-0.6}$ .

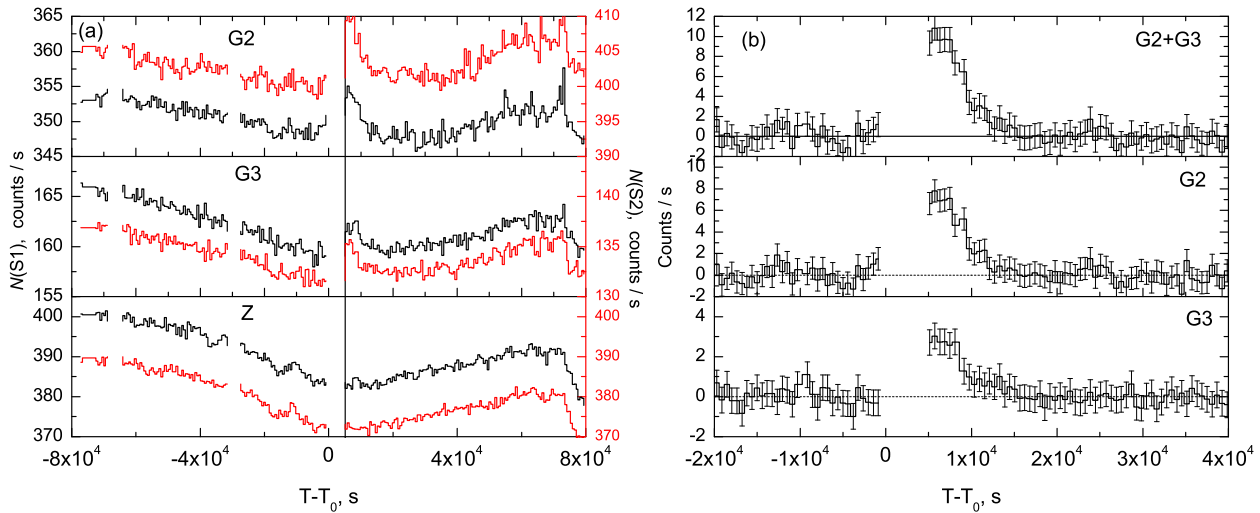


Fig. 15.— Record of the background summed over 800 s in the G2, G3, and Z windows.  $T_0$  corresponds to the Konus-Wind trigger time. (a) The data recorded on December 27–28, 2004. The count rates recorded by the S1 (dark curve) and S2 (light curve) detectors are given for each window. The gaps in the record correspond to the data output intervals after the completion of the trigger record. The vertical bar marks the record resumption time after the output of trigger data on the giant flare. (b) A segment of the record near the giant flare – the record in the G2 and G3 windows, the count rates were averaged over the two detectors (the background was subtracted,  $1\sigma$  errors of the measured count rates are given).

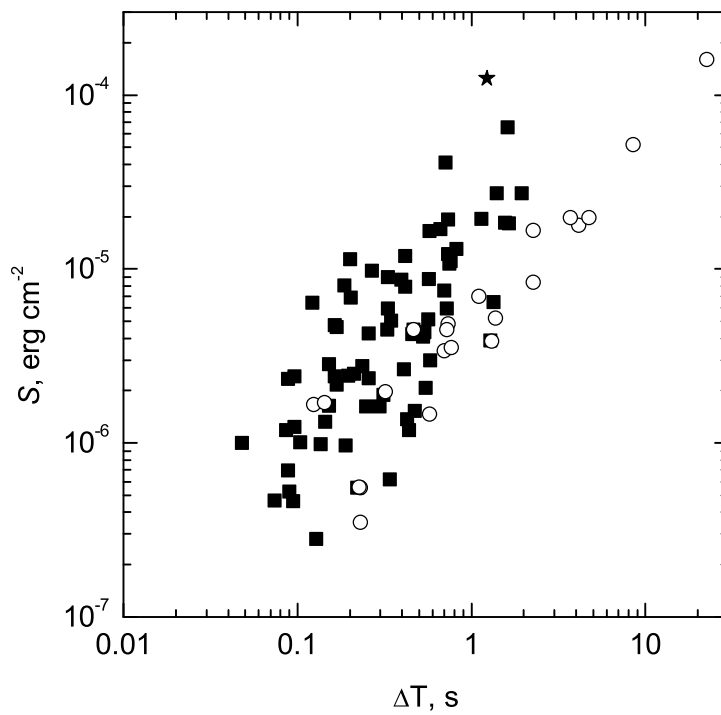


Fig. 16.—  $S$ - $\Delta T$  diagram for the trigger recurrent bursts detected by Konus-Wind and Helicon-Coronas-F before (filled squares; 72 bursts) and after (open circles; 22 bursts) the giant flare on December 27, 2004 (the series of bursts are not included). The asterisk marks the precursor of the giant flare.

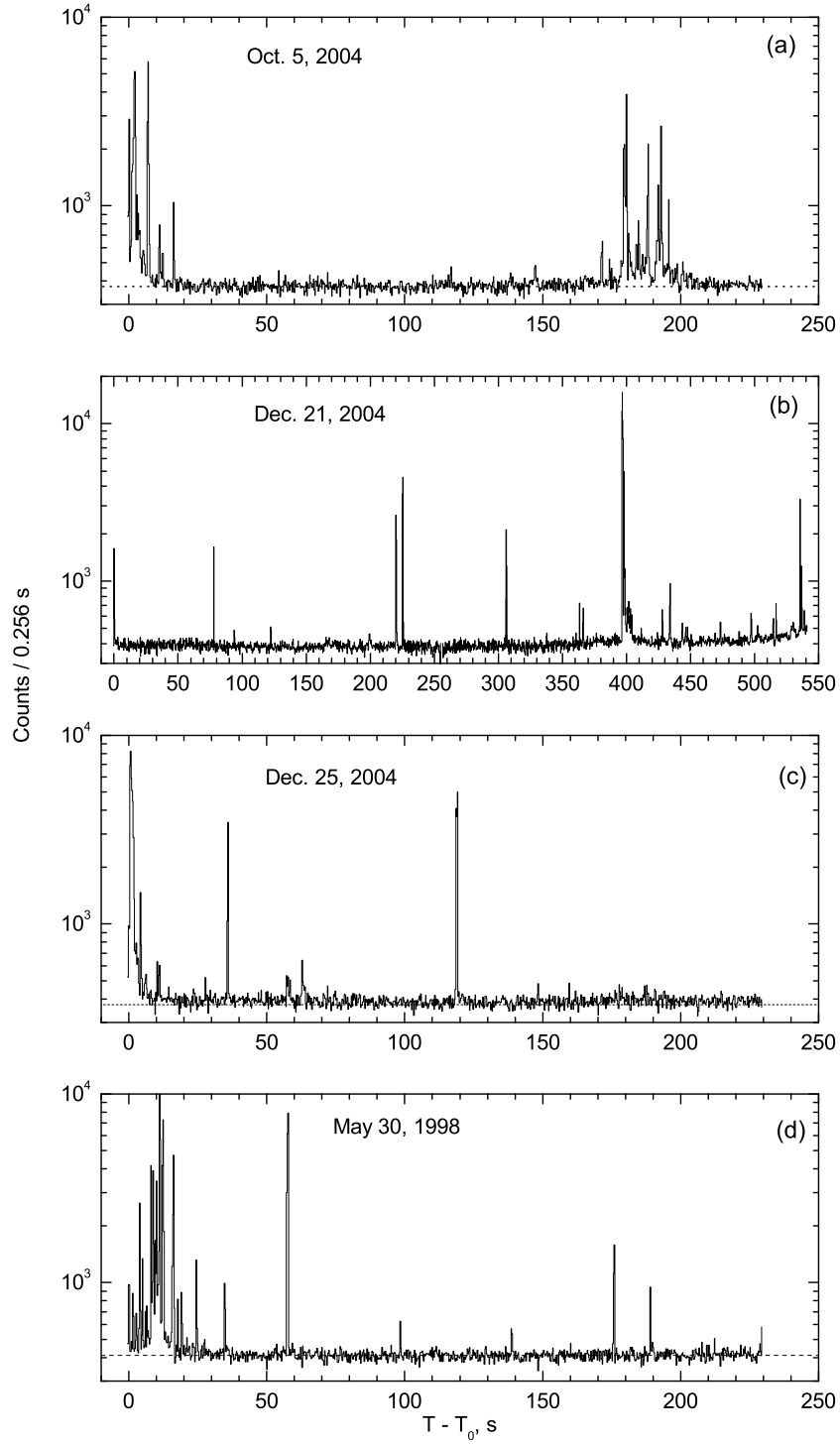


Fig. 17.— Time histories of the series of bursts in SGR 1806-20 (a, b, c) and SGR 1900+14 (d). The fluence in the range 20–200 keV is  $7.6 \times 10^{-5}$  (a),  $3.3 \times 10^{-5}$  (b),  $7.6 \times 10^{-5}$  (c), and  $5.9 \times 10^{-5}$  erg cm $^{-2}$  (d).

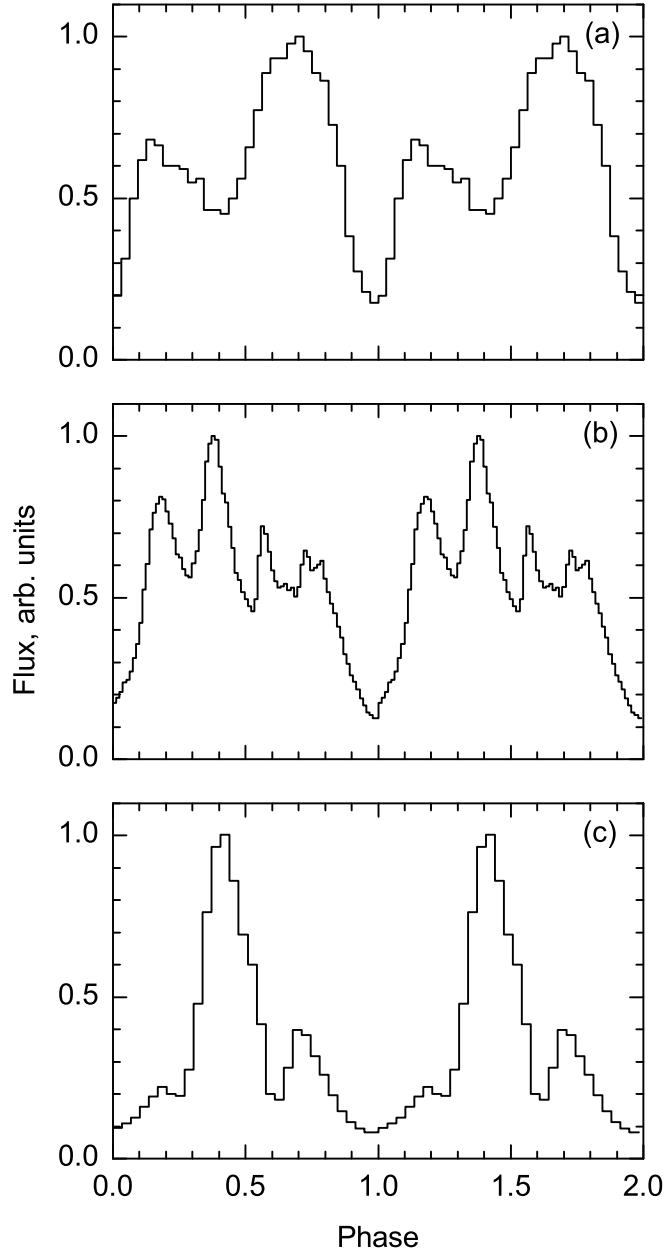


Fig. 18.— Phase-averaged profiles of the pulsating tails of the three giant flares from SGRs: (a) on March 5, 1979, from SGR 0526-66 (Venera-11 and Venera-12 data), (b) on August 27, 1998, from SGR 1900+14 (Konus-Wind data), and (c) on December 27, 2004, from SGR 1806-20 (Konus-Wind data).